^{29}Si hyperfine structure of the P_{b1} interface defect in thermal $(100)Si/SiO_2$

1998 J. Phys.: Condens. Matter 10 L465

(http://iopscience.iop.org/0953-8984/10/27/004)

J. Phys.: Condens. Matter **10** (1998) L465–L472. Printed in the UK PII: S0953-8984(98)93843-7

LETTER TO THE EDITOR

^{29}Si hyperfine structure of the P_{b1} interface defect in thermal (100)Si/SiO_2

A Stesmans, B Nouwen and V V Afanas'ev

Department of Physics, University of Leuven, 3001 Leuven, Belgium

Received 30 April 1998

Abstract. The observation of the electron spin resonance hyperfine (hf) spectra associated with the unpaired electron of the P_{b1} interface defect in thermal (100)Si/SiO_2 shows that the dominant interaction arises from a single ^{29}Si isotope. The hf tensor displays weakly monoclinic *I* (nearly axial) symmetry, with the principal axes of the *g* and hf tensors coinciding. A molecular orbital analysis indicates that the unpaired electron resides for ∼58% in a single unpaired Si hybrid orbital, found to be 14% s-like and 86% p-like, with the p-orbital markedly pointing closely along a ⟨211⟩ direction at 35.26° with the [100] interface normal. With oxygen not constituting an immediate part of the defect, the results firmly establish the key part of the P_{b1} defect as a tilted (∼20° about ⟨011⟩) $Si_3{\equiv}Si\cdot$ unit.

Thermal oxidation of Si is accompanied by the inherent generation of defects at the Si/SiO_2 interface [1, 2]. A particular class are the mismatch induced paramagnetic point defects, referred to as P_b-type centres [2] as detected by electron spin resonance (ESR). At least part of these were shown to be electrically active as trapping and/or recombination centres [3] thus impairing crucial currents in adjacent Si layers, which explains the high technological interest in atomic identification. Their appearance depends on the crystallographic interface orientation [2]. At the (111)Si/SiO_2 interface, ESR has so far isolated only one type of defect, specifically termed P_b, exhibiting C_{3v} symmetry. It has been identified [2, 4, 5] as a trivalent interfacial Si backbonded to three Sis in the substrate, denoted as $Si_3{\equiv}Si\cdot$, where the dot symbolizes the unpaired electron in an $sp^3_{\langle 111\rangle}$-like orbital. Generally, only the defect orientation with $sp^3_{\langle 111\rangle}$ along the [111] interface normal is observed [6].

The (100)Si/SiO_2 interface, by contrast, exhibits two prominent types of defects, termed P_{b0} and P_{b1}. For standard oxidation temperatures (800–950 °C), the naturally incorporated densities are [7] $[P_b] \sim 5 \times 10^{12}$ cm^{-2} and [8] $[P_{b0}]$, $[P_{b1}] \sim 1 \times 10^{12}$ cm^{-2}. The initial observations [5] indicated lower than C_{3v} symmetry (C_{2v})—monoclinic *I*—for both defects, the P_{b0} symmetry however being nearly axial about ⟨111⟩. Based on the close ESR features, P_b and P_{b0} were suggested to be similar: one opinion now is that P_{b0} also concerns a ⟨111⟩ oriented $\cdot Si{\equiv}Si_3$ but residing at steps or ⟨111⟩ Si/SiO_2 microfacets at the macroscopic (100)Si/SiO_2 interface [9, 10]. It would thus merely be a testimony for the amount of crystallographically non-ideal (100)Si termination.

As to P_{b1}, the initially proposed model by Poindexter *et al* [5] was an interfacial $\cdot Si{\equiv}Si_2O$ entity (cf P^P_{b1} model in figure 1), suggesting the centre to differ chemically from P_b and P_{b0}. That model, however, had appeared untenable partly on experimental, but mainly on theoretical grounds [11]. The latter was concluded from detailed calculations on five model clusters, including the initial $\cdot Si{\equiv}Si_2O$ model and the SB1 model—the latter

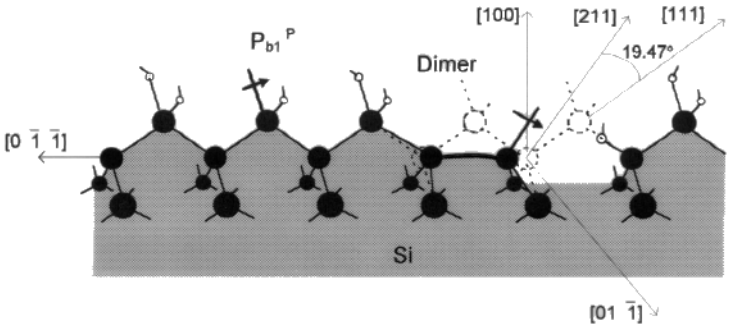

Figure 1. Models for P_{b1} at the (100) Si/SiO_2 interface: (*a*) initial model (P^P_{b1}) after [5]; (*b*) strained defected Si–Si dimer (similar to SB1 model in [11]) with unpaired sp^3 hybrid adjusted along [211]. Dashed drawing pictures the Si lattice before the dimer formation. Open and solid circles represent O and Si atoms, respectively.

symbolizing an unpaired Si bond at one end of a strained reconstructed interfacial Si–Si dimer, i.e., $Si_2 = Si^{\cdot}$—$Si \equiv Si_2O$, where the long hyphen represents the strained bond. The model originated from the Si–Si dimer being pictured as a natural strain-relief site necessary to absorb strain [12, 13] in matching a-SiO_2 to (100)Si. None of the models appeared acceptable. Up to now, the atomic identity of P_{b1} is still unknown. Actually, the basic reason for this is that, due to enhanced experimental difficulty, the available set of ESR data is incomplete, often unclear. Particularly missing is solid information on hyperfine (hf) structure, i.e., interaction of the unpaired defect electron with nearby magnetic nuclei. Indeed, it is well known in ESR spectroscopy that in addition to other ESR parameters, conclusive point defect identification must come from hf structure.

Recent work [9] on (100)Si/SiO_2 structures exhibiting predominantly the P_{b1} species

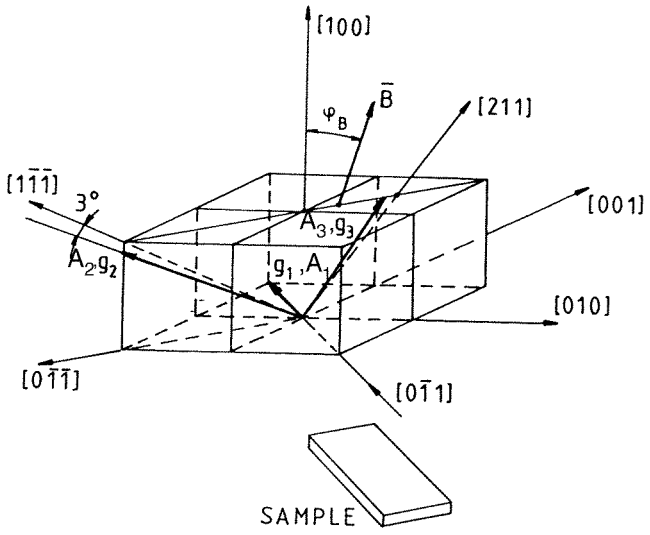

Figure 2. P_{b1} g and hf tensor (A) principle axes within the cubic Si lattice for one of the four interface restricted equivalent defect orientations at the (100)Si/SiO_2 interface. Also shown is the applied sample geometry.

resulted in accurate values of P_{b1} ESR parameters. The monoclinic I symmetry of the g tensor was confirmed with $g_1 = 2.0058$, $g_2 = 2.007\,35$ and $g_3 = 2.0022$, where, importantly, the g_3 direction is at $3 \pm 1^\circ$ (towards the [100] interface normal $\boldsymbol{n}$) with a $\langle 211 \rangle$ direction (cf figure 2). Only the four crystallographic defect orientations (ESR) equivalent through $\bar{4}$ [100] face symmetry occur. From these results together with previous salient ESR data, the key part of P_{b1}, like P_b and P_{b0}, was also pictured as a single unpaired sp^3 hybrid on an interfacial Si. Furthermore, the former improved results on g tensor and field angle dependent line broadening included a slight hint that the unpaired hybrid would point along the g_3 direction, i.e., closely along [211], instead of the g_2 direction (close to a normal $\langle 111 \rangle$ direction). But in the absence of supportive hf identification, the hint necessarily remained as speculative as uncertain.

There has so far only been one report of successful P_{b1} hf observation. In a pioneering work [14] on standard thermal (100)Si/SiO_2, a single (only for the applied magnetic field $\boldsymbol{B} \| \boldsymbol{n}$) hf observation was reported for both P_{b0} and P_{b1}, tentatively attributed to ^{29}Si hf interaction. A hf splitting of $A_{[100]} \sim 157$ G was reported for P_{b1}, about 50 G larger than for P_{b0} ($\sim$105 G for $\boldsymbol{B} \| \boldsymbol{n}$) which in turn is comparable to the one of P_b ($\sim$117 G for $\boldsymbol{B} \| \boldsymbol{n}$). From this, the P_{b1} hf structure was speculated also to arise from interaction with a single ^{29}Si, as is the case for P_{b0} and P_{b1}, leading to the conclusion that the P_{b1} unpaired electron is also highly localized on one Si atom. Although useful, the singularity of this observation left any progress in modelling desperately speculative, the modelling feeling tempted to infer farther reaching conclusions than allowed by experimental facts. Moreover, that hf observation was recently stoutly contested [15] by ESR results on porous Si.

Clearly, P_{b1} identification fails because of the lack of hf structure information. This is the subject of the current work, reporting on the successful determination of the hf tensor (A) symmetry and interaction strengths of the dominant ^{29}Si hf structure, providing a fundamental clue to the defect's microscopic structure.

ESR-compatible samples of 2×9 mm^2 main face were cut from a commercial 4 inch diameter two side polished (100)Si wafer (float zone; $\sim$0.1 Ω cm; p-type) about 29 μm thick, with the 9 mm edge along a $\langle 011 \rangle$ direction. After cleaning, the samples were submitted to three thermal steps: (1) Thermal oxidation at 970 °C (1.1 atm O_2; 99.9995%; dry; $d_{ox} \sim 42$ nm); (2) hydrogenation (H_2; 99.9999%; 1 atm) at 795 °C for 1 h; (3) as after such a step, the major part of the P_b-type defects are left passivated by H (i.e., $P_{b(0,1)}H$ formation), this was finally followed by a vacuum anneal at $\sim$620 °C for $\sim$1 h—a treatment known to exhaustively depassivate (ESR-activate) the P_b-type defects [8, 16]. Typically, an intensity ratio $[P_{b1}]/[P_{b0}] \approx 1.22$ is obtained, with $[P_{b1}] = (7.2 \pm 0.5) \times 10^{12}$ cm^{-2}. All the thermal steps were terminated by cooling to room temperature ($\sim$20 min) in unaltered ambient. An ESR sample bundle typically comprised about 70 slices.

ESR measurements were carried out in the 1.6–3.4 K range employing a CW K-band ($\sim$20.09 GHz) spectrometer [7]. Routinely, it is operated in the adiabatic slow passage (incident microwave power $P_\mu \leqslant 20$ pW) absorption mode, where first derivative absorption signals were recorded by modulation ($\sim$100 kHz; amplitude $\sim$ 0.6 G) of $\boldsymbol{B}$. Optimum hf structure detection, however, was obtained at higher P_μ ($\sim$0.8 nW). The rapid passage effects at 1.6 K under these partial saturation conditions resulted in recording undifferentiated absorption-like peaks. $\boldsymbol{B}$ was rotated in the (011) plane with ϕ_B, the angle of $\boldsymbol{B}$ with $\boldsymbol{n}$, varying from 0 to 90°. Typically, the spectra were averaged over 100 to 200 scans.

Typical ESR spectra observed in the low P_μ (undistorted) mode at 1.6 K are shown in figure 3 for two orientations of $\boldsymbol{B}$. Though this detection mode is not the most sensitive one (not used generally for hf structure mapping), hf structure is clearly resolved next to strong P_{b0} and P_{b1} (central) Zeeman signals. The simplest spectrum occurs for $\boldsymbol{B} \| \boldsymbol{n}$, displaying

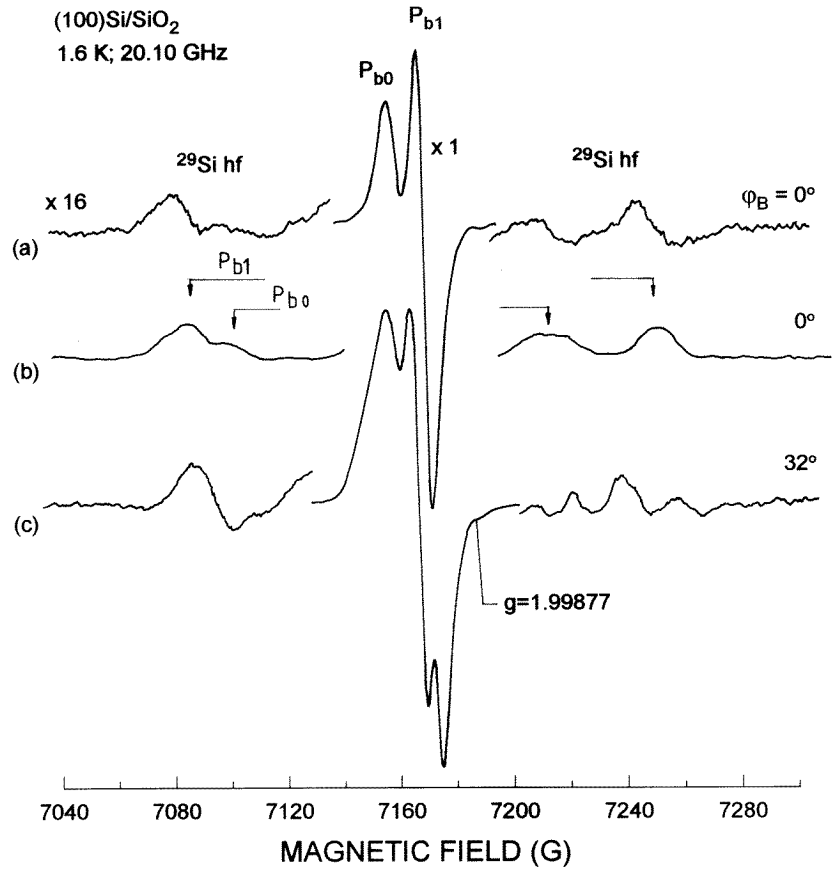

Figure 3. Absorption derivative ESR spectra observed in the adiabatic slow ((*a*), (*c*) $P_\mu \sim 20$ pW) and rapid ((*b*) $P_\mu \sim 0.8$ nW) passage mode in thermal (100)Si/SiO_2 for two directions of $\boldsymbol{B}$ in the (011) plane. They are comprised of the P_{b0} and P_{b1} Zeeman signals and resolved ^{29}Si hf structure. The angular dependent P_{b1} hf structure is clearly exposed.

pairs of hf doublets of splitting $\Delta B_{hf}[100] = 105 \pm 2$ and 156 ± 2 G centred at the P_{b0} and P_{b1} Zeeman signals, respectively. The first one is the expected P_{b0} ^{29}Si hf structure, of splitting well in agreement with previous results [14, 17]. The second doublet is assigned to P_{b1}. It was observed once before, with identical splitting [14]. In the latter work, to maximize the signal-to-noise (S/N) ratio, ESR was measured at <30 K in the dispersion mode under fast passage conditions giving absorption-like signals. When measuring at higher P_μ under similar circumstances, our hf spectrum for $\boldsymbol{B} \| \boldsymbol{n}$ (with enhanced S/N ratio) becomes indeed virtually identical to the one of Brower (figure 4 of [14]), as shown in figure 3(b), thus confirming that observation.

Unlike previous work, the achieved signal enhancement has enabled us to perform the full angular variation of the hf structure. This is exemplified in figure 3 also, where the P_{b1} hf structure is seen to split into various, generally three, components. This is as expected for P_{b1} as for $\boldsymbol{B}$ rotating in the (011) plane, the g map exhibits three branches. The three P_{b1} hf components exhibit different relative intensity, one being of approximately double intensity. Anticipating the interpretation, this factor was incorporated in the P_{b1} hf mapping through using different symbols for the hf lines of estimated double intensity.

Next to the hf spectral composition and magnitudes of observed splittings, a key element in assigning hf structure is the relative signal intensity. As determined on undistorted low P_μ spectra, the ratio in spectral intensity (area under absorption curve) of the hf doublet to the Zeeman signal is found to be 0.044 ± 0.006 for P_{b1}. This agrees with the value of 0.049 expected for interaction with a single ^{29}Si (4.70% natural abundance) nucleus.

Although the P_{b0} hf signals are less prominent for various reasons, its hf tensor was also determined. In agreement with previous reports [17, 18], it is found axially symmetric about $\langle 111 \rangle$ with $A_\parallel = 149 \pm 4$ and $A_\perp = 75 \pm 5$ G.

The entire P_{b1} spectrum can be described [19] by the simplified spin Hamiltonian

$$\mathcal{H} = \mu_B \boldsymbol{B} \cdot \boldsymbol{g} \cdot \boldsymbol{S} + \boldsymbol{I}_j \cdot \boldsymbol{A}_j \cdot \boldsymbol{S} \tag{1}$$

with effective electron spin $S = \frac{1}{2}$. The first term is the electronic Zeeman interaction, the second term the spin–nucleus hf interaction. Here $\boldsymbol{g}$ is the electronic g dyadic, I the nuclear spin ($= \frac{1}{2}$ for ^{29}Si) and $\boldsymbol{A}_j$ the hf tensor for interaction of the electron spin with the jth nearby lattice site; for the present P_{b1} case, $j = 1$. Similar to the Zeeman g map, the hf structure pattern is found to be readily fitted with monoclinic I symmetry, with the relative branch intensities in agreement with experimental data. The optimised fitting gives the principal hf tensor values A_1 ($\parallel [0\bar{1}1] = 102 \pm 3$ G, A_2 ($\sim\parallel [111]$) $= 112 \pm 3$ G and A_3 ($\sim\parallel [211]$) $= 167 \pm 3$ G. The departure from trigonal (axial) symmetry thus appears small. In fact, within experimental accuracy, the data are equally well fitted by axial symmetry, giving the values (see table 1) $A_\parallel = A_3 = 167$ G and $A_\perp = 107$ G ($= (A_1 + A_2)/2$). To ease the discussion, we shall henceforth assume axial symmetry. The principal hf tensor axes are found identical with those of the g tensor, which need not *a priori* be so (*vide infra)*. However, while a satisfactory fit is obtained, the experimental accuracy does not permit us to specify the principal A tensor directions to better than $\sim 3^\circ$.

Table 1. ^{29}Si hyperfine interaction parameters of the P_b and P_{b1} defects in bulk thermal (111) and (100)Si/SiO_2. The MO wave function coefficients were calculated [19] using $|\Psi_{3s}(0)|^2 = 34.55 \times 10^{-24}$ cm^{-3} and $\langle r_{3p}^{-3} \rangle = 17.78 \times 10^{-24}$ cm^{-3} [20].

Defect	Reference	$A_\parallel$ (G)	$A_\perp^{a}$ (G)	$A_{B\parallel[100]}$ (G)	hf axis	No of equivalent sites	α^2	β^2	η^2
P_b	[3]	156 ± 5	91 ± 9	117	[111]	1	0.11	0.89	0.62
P_{b1}	current work	167 ± 3	107 ± 4	156 ± 2	$\angle$[211], $A_\parallel = 3^\circ$	1	0.14	0.86	0.58

[a] Fitting monoclinic I symmetry results in $A_1(\parallel [0\bar{1}1]) = 102 \pm 3$ G, $A_2(\sim\parallel [111]) = 112 \pm 3$ G, and $A_3 = A_\parallel$.

Following the linear combination of atomic orbitals (LCAO) analysis [19], the P_{b1} unpaired electron may be represented by the molecular orbital (MO) wave function $|\psi(\boldsymbol{x})\rangle = \sum_i \eta_i(\alpha_i|\psi_{s,i}\rangle + \beta_i|\psi_{p,i}\rangle)$, where η_i gives the localization of the hybrid at the ith site. The results for the MO parameters are compared with those of P_b in table 1. This provides interesting information: (i) it tells us that 58% of the paramagnetic orbital is localized on a single Si atom at the interface with the hybrid exhibiting 14% s and 86% p character. These hybrid values are quite similar to those found for prototype Si dangling bond defects such as, e.g., G8 (p-vacancy centre) [19] and P_b (cf table 1), demonstrating that the P_{b1} paramagnetic orbital also concerns a single Si dangling bond orbital. (ii) Perhaps most revealing is that this unpaired Si hybrid points closely (within $\sim 3^\circ$) along a $\langle 211 \rangle$

direction at 35.26° with $\boldsymbol{n}$. (iii) The gyromagnetic and hf tensor symmetries are found identical within experimental accuracy. But, as mentioned, the accuracy on this statement cannot be better than ±3°. However, to simplify the wording, we shall henceforth assume both tensor symmetries coinciding.

Within the LCAO framework, the results must imply that the key part of P_{b1} consists of a tilted ≡Si· entity that, under interfacial physicochemical influence, has rotated about a [011] axis over ∼20° so as to bring the Si dangling bond from its normal [111] direction towards the nearest [211] direction (cf figure 2).

This finding on the unpaired sp^3-like hybrid direction makes previous results [9] transparent. First, there are the measured g shifts $\Delta g \equiv g - g_{fe}$, where $g_{fe} = 2.002\,32$ is the free electron g value. The shift is smallest, i.e., $-0.000\,12$ (close to zero), along the [211] g_3 principal direction, while the shift is substantially larger and of comparable magnitude (i.e., 0.005 and 0.0035) along the other two principal g directions. Well in line with the current finding that the unpaired P_{b1} hybrid points along the g_3 direction, the successful g shift interpretation for a single broken Si orbital based on simple MO theory [19] indeed predicts to first order zero g shift for $g_\parallel$ and a positive, order of magnitude larger shift in $g_\perp$. Second, the inferred dangling bond direction (g_3 direction) is also corroborated by the recently revealed strain induced angular dependent part in the P_{b1} linewidth [9]. It was found smallest (possibly absent) along the g_3 direction. This again is consonant with the simple MO view [19], predicting that, to first order, the strain induced variations in bond lengths and angles near the defect site only lead to a distribution in $g_\perp$, none in $g_\parallel$, however, hence also minimal broadening along the sp^3 hybrid (g_3) direction.

With the basic atomic entity of P_{b1} identified, it then remains to model how the unit is incorporated in a larger defect structure. When placed then in an appropriate sufficiently extended Si/SiO_2 cluster, detailed quantum-mechanical calculation will enable thorough theoretical verification. The defect modelling can only be considered definite after successful theoretical back up. Together with the newly gained hf information, this search should be based on the salient experimental facts, mostly inferred by ESR. Salient P_{b1} facts include: (i) the P_{b1} g tensor data show that P_{b1} is an interface constrained defect of monoclinic I symmetry [5, 9]. The lowest principal g value $g_3 = 2.0022$ is only weakly shifted from g_{fe}. This g_3 axis is at $3 \pm 1°$ (towards the interface normal) with a ⟨211⟩ direction at 54.74° with the (100) interface plane, while the principal g_2 (= 2.007 35) direction is at 3° with ⟨111⟩. (ii) The magnetic angle dependent line broadening [9], ascribed to a strain induced distribution predominantly in $g_\perp$, is smallest (absent) for $\boldsymbol{B} \| g_3$ axis [211]. (iii) The P_{b1} centre is more sensitive to saturation than P_{b0}— ∼3 times in terms of P_μ. (iv) The study [14] of ^{17}O enriched (100)Si/SiO_2 indicates that O is not an immediate part of the P_{b1} defect. With no hydrogen hf observed, H is also excluded as a building block of the defect. (v) The activation energy E_a for passivation in molecular H was found [12] close for all three defects P_b, P_{b0} and P_{b1}, i.e., $E_a(P_b, P_{b0}) = 1.51 \pm 0.04$ eV, and $E_a(P_{b1}) = 1.57 \pm 0.04$ eV. (vi) Though in dispute [3], the centre was recently concluded [8] not to be active as an electrical interface trap, implying that there are no $+/0$ and $0/-$ charge transition levels deep in the Si gap.

Perhaps in a simplest scheme, it may be pictured as incorporated as one half of a $Si_2 = Si\cdot\text{–}Si \equiv Si_3$ defected dimer configuration (similar to SB1). As a result of the pulling of the two interfacial next nearest-neighbour Si atoms together under influence of surrounding strain during the Si–Si bond reformation, the $Si_2 = Si\cdot$— moiety with the left broken bond may be envisaged as having tilted over ∼20° about the $[0\bar{1}1]$ axis away from [111] towards the [100] interface normal, the unbonded hybrid now pointing approximately along [211] (see figure 1). In this picture then, the fact that the g_2 axis direction ends up nearly along

[111] is rather coincidental. Placed slightly subinterfacial, the defect structure thus being rigorously fixed by the Si lattice without much disturbance from the top SiO_2 network, this picture could, at least in principle, incorporate the various salient experimental facts thus far accumulated: the symmetry axes of the unpaired orbital at such a tilted $Si_2 = Si^{\cdot}$— entity, i.e., $[0\bar{1}1]$, ∼[211] and ∼ $[1\bar{1}\bar{1}]$, agree with the measured principal g axes. Also according to this symmetry, with one backbond strained, three different principal g value magnitudes are expected, that is, lower than axial symmetry. Since the unpaired sp^3-like hybrid points along the g_2 axis (∼[211]), the g shift along [211] should be an order of magnitude smaller than along the two other perpendicular directions, as observed. As the unpaired spin resides in a single dangling sp^3-like hybrid, the g and hf tensor symmetries are expected to coincide to first order, also as observed. However, as mentioned, initial calculations [11] concluded the $Si_2{=}Si^{\cdot}{-}Si \equiv Si_2O$ dimer model to be untenable. Perhaps, improved calculations on a more representative cluster incorporating the dimer at a subinterfacial level (cf figure 1) may provide more insight. But however attractive this picture, other structures may be envisaged.

Based on symmetry considerations, also of interest is the $Si_2{=}Si^{\cdot}{-}O{-}Si \equiv Si_2O$ oxygen bridge strain relief centre (termed SB2 in [11]). Like the dimer, it is also considered as a natural strain relief centre [12, 13] in matching c-Si to a periodic form (e.g., tridymite) of SiO_2. Based on symmetry properties, even the initial P_{b1}^{P} model may be reconsidered. Yet, while both models may display an acceptable symmetry, they are likely untenable on grounds of theoretical calculations [11] of the electric level positions in the Si band gap and the incorporation of O as an essential building block (O backbond).

In summary, optimized ESR experiments have succeeded in the full angular mapping of the strong ^{29}Si P_{b1} hf interaction in thermal (100)Si/SiO_2. The data demonstrate that the hf structure results from interaction with a single ^{29}Si isotope, the paramagnetic P_{b1} electron being localized for ∼58% in a single sp^3 hybrid approximately pointing along a ⟨211⟩ direction at 35.26° with the [100] interface normal. The P_{b1} defect is convincingly identified, like P_b, as a prototype Si dangling bond ($\equiv Si\cdot$) defect. If excluding O as a basic building block of the defect, its basic entity is revealed as a ⟨211⟩ oriented (∼20° tilted) strained $Si_3 \equiv Si\cdot$ unit. Clearly, to trace the way this unit is incorporated in a larger defect structure, thorough theoretical analysis is essential. It is felt that with the currently provided hf data, this can now reliably be performed so as to culminate in the definite model.

The results complete the identification of the ESR-active defects at the Si/SiO_2 interface. With inclusion of the similarity of P_{b0} and P_{b1}, it now appears that the kernel of all three defects, P_b, P_{b0} and P_{b1}, is *chemically* identical, i.e., $\cdot Si \equiv Si_3$ is the generic entity of the three defects. Yet, they clearly do differ *physically*.

References

[1] For a review on Si/SiO_2 defect physics, see the 13 papers in 1989 *Semicond. Sci. Technol.* **4** 961, and references therein

[2] Poindexter E and Caplan P 1983 *Prog. Surf. Sci.* **14** 211
Helms R and Poindexter E 1994 *Rep. Prog. Phys.* **57** 791

[3] Gerardi G J, Poindexter E H, Caplan P J and Johnson N M 1986 *Appl. Phys. Lett.* **49** 348

[4] Brower K 1983 *Appl. Phys. Lett.* **43** 1111

[5] Poindexter E, Caplan P, Deal B and Razouk R 1981 *J. Appl. Phys.* **52** 879

[6] Stesmans A 1986 *Appl. Phys. Lett.* **48** 972

[7] Stesmans A 1993 *Phys. Rev.* B **48** 2418

[8] Stesmans A and Afanas'ev V V 1998 *J. Phys.: Condens. Matter* **10** L19

[9] Stesmans A and Afanas'ev V V 1998 *J. Appl. Phys.* **83** 2449

[10] von Bardeleben H J, Schoisswohl M and Cantin J L 1996 *Colloids Surf.* A **115** 277

[11] Edwards A H 1988 *The Physics and Chemistry of SiO_2 and the SiO_2 interface* ed C R Helms and B E Deal (New York: Plenum) p 271
[12] Ourmazd A, Taylor D W, Rentschler J A and Bevk J 1987 *Phys. Rev. Lett.* **59** 213
[13] Pasquarello A, Hybertson M S and Car R 1995 *Phys. Rev. Lett.* **74** 1024
[14] Brower K L 1987 *Z. Phys. Chem., NF* **151** 177
[15] Cantin J L, Schoisswohl M, von Bardeleben H J, Zoubir N H and Vergnat M 1995 *Phys. Rev.* B **52** R11 599
[16] Brower K L 1990 *Phys. Rev.* B **42** 3444
[17] Carlos W E 1987 *Appl. Phys. Lett.* **50** 1450
[18] Gabrys J W, Lenahan P M and Weber W 1993 *Microelectr. Eng.* **22** 273
[19] Watkins G D and Corbett J W 1961 *Phys. Rev.* **121** 1001
Watkins G D and Corbett J W 1964 *Phys. Rev.* **134A** 1359
[20] Morton J R and Preston K F 1978 *J. Magn. Res.* **30** 577
[21] Stesmans A 1996 *Appl. Phys. Lett.* **68** 2076
Stesmans A 1996 *Appl. Phys. Lett.* **68** 2723